AD-A150 296 RESEARCH EFFORTS IN SUPPORT OF RESONANCE EXTRACTION STUDIES VOLUME 1 IMPR..(U) GENERAL RESEARCH CORP SANTA BARBARA CA J R AUTON ET AL. NOV 84 GRC-CR-84-1309 1/1

UNCLASSIFIED N00014-80-C-0299 F/G 20/14 NL

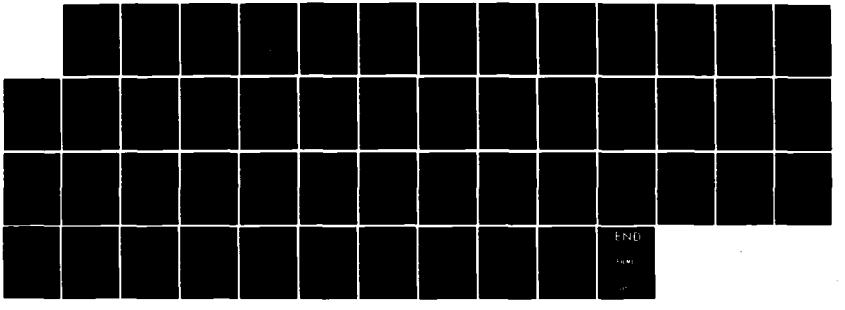

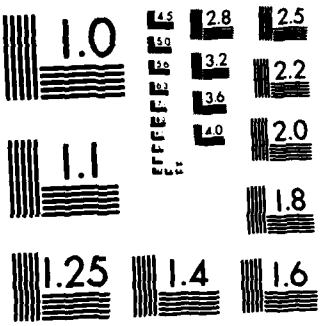

CR-84-1319

Research Efforts In Support of Resonance Extraction Studies

Volume I

Improvement and Validation of TWFD: A Thin-Wire Frequency-Domain Scattering Code

by
T. L. Larry
J. R. Auton
M. L. VanBlaricum

November 1984

ADVANCED TECHNOLOGIES DIVISION

GENERAL RESEARCH CORPORATION

P.O. BOX 6770, SANTA BARBARA, CALIFORNIA 93160-6770

Prepared for:

Office of Naval Research
800 North Quincy Street
Arlington, VA 22217

Final Report
On ONR Contract No. N00014-80-C-0299

UNCLASSIFIED

SECURITY CLASSIFICATION OF THIS PAGE (When Data Entered)

REPORT DOCUMENTATION PAGE	READ INSTRUCTIONS BEFORE COMPLETING FORM
1. REPORT NUMBER	2. GOVT ACCESSION NO. A150296 / 3. RECIPIENT'S CATALOG NUMBER
4. TITLE (and Subtitle) RESEARCH EFFORTS IN SUPPORT OF RESONANCE EXTRACTION STUDIES, VOLUME I, IMPROVEMENT AND VALIDATION OF TWFD: A THIN-WIRE FREQUENCY-DOMAIN SCATTERING CODE	5. TYPE OF REPORT & PERIOD COVERED: Final Report 10/1/82 - 9/30/83
	6. PERFORMING ORG. REPORT NUMBER: CR-84-1309
7. AUTHOR(s): J. R. Auton, T. L. Larry, M. L. VanBlaricum	8. CONTRACT OR GRANT NUMBER(s): N00014-80-C-0299
9. PERFORMING ORGANIZATION NAME AND ADDRESS: General Research Corporation, P.O. Box 6770, Santa Barbara, CA 93160-6770	10. PROGRAM ELEMENT, PROJECT, TASK AREA & WORK UNIT NUMBERS
11. CONTROLLING OFFICE NAME AND ADDRESS: Office of Naval Research, 800 North Quincy Street, Arlington, VA 22217	12. REPORT DATE: November 1984 / 13. NUMBER OF PAGES: 43
14. MONITORING AGENCY NAME & ADDRESS (if different from Controlling Office)	15. SECURITY CLASS. (of this report): UNCLASSIFIED / 15a. DECLASSIFICATION DOWNGRADING SCHEDULE
16. DISTRIBUTION STATEMENT (of this Report): This document has been approved for public release and sale; its distribution is unlimited.	
17. DISTRIBUTION STATEMENT (of the abstract entered in Block 20, if different from Report)	
18. SUPPLEMENTARY NOTES	
19. KEY WORDS (Continue on reverse side if necessary and identify by block number): SEM, Frequency Domain; MOM, Integral Equation; RCS, Radar Cross Section; Thin Wire	
20. ABSTRACT (Continue on reverse side if necessary and identify by block number): This report presents the modification and validation of a thin-wire frequency-domain (TWFD) method of moments code for scattering calculations. The code also can produce the natural resonances. The code was validated with measurement data.	

DD FORM 1 JAN 73 1473 EDITION OF 1 NOV 65 IS OBSOLETE

UNCLASSIFIED

SECURITY CLASSIFICATION OF THIS PAGE (When Data Entered)

CR-84-1319

Research Efforts In Support of Resonance Extraction Studies

Volume I

Improvement and Validation of TWFD: A Thin-Wire Frequency-Domain Scattering Code

by
T. L. Larry
J. R. Auton
M. L. VanBlaricum

November 1984

ADVANCED TECHNOLOGIES DIVISION

GENERAL RESEARCH CORPORATION
P.O. BOX 6770, SANTA BARBARA, CALIFORNIA 93160-6770

Prepared for:
Office of Naval Research
800 North Quincy Street
Arlington, VA 22217

Final Report
On ONR Contract No. N00014-80-C-0299

TABLE OF CONTENTS

LIST OF ILLUSTRATIONS

LIST OF ILLUSTRATIONS
(Continued)

LIST OF TABLES

1.0 INTRODUCTION

The development of a thin-wire frequency-domain (TWFD) method of moments code was discussed in a previous report [1]. Since that time this code has undergone further development and numerical testing. The purpose of the code is to provide a theoretical and numerical basis to aid in understanding the resonance region electromagnetic scattering from thin-wire stick models. This frequency domain code augments a time-domain code (TWTD) which calculates the scattered transient response for an impulsive incident field. The outputs from both of these codes have provided numerical predictions which have been indispensible in assessing our ability to extract resonance information from actual scattering range data.

The Laplace transform $H(s,\Omega)$ of a target's impulse response can be expressed as [2]

$$H(s,\Omega) = \sum_{i=1}^{N} \frac{A_i(\Omega)}{s-s_i} + W(s,\Omega) \quad . \tag{1}$$

The directions and polarizations of the incident and scattered fields are collectively denoted by Ω in the above. The Fourier transform $H(\omega,\Omega)$ of the impulse response is simply $H(s,\Omega)$ evaluated along the $j\omega$ axis. The summation on the right side of equation (1) includes all resonance modes which contribute significantly to the sattering. The pole positions s_i are independent of Ω whereas the corresponding residues A_i dependent on Ω. The entire function portion, $W(s,\Omega)$, of the response contains valuable non-resonance information about the target.

For a specified stick model the TWFD code has been designed to perform the following basic functions:

1) Locate the positions s_i of the resonance poles.

2) Calculate the corresponding residues A_i for the specified values of Ω.

3) Directly calculate the transfer function $h(\omega,\Omega)$ for specified values of Ω.

These capabilities allow us to do a variety of numerical experiments which can be compared with TWTD [3] numerical experiments as well as with the results of analyzing physical measurements. Each of these capabilities will be discussed in this report. Following that we will show the results of some numerical experiments which were performed using TWFD on a particular thin-wire model. These then are compared with results using TWTD as well as with physical measurements made with the same model.

2.0 SUMMARY OF TWFD CODE

The TWFD code solves for the cw scattering by using the method of moments. This section will summarize the formulation TWFD uses to solve the frequency domain problem. Reference [1] provides most of the details. The following three sections will concentrate on the primary capabilities we have built into the code since that report.

The scattered cw field can be obtained by applying a Green's function to the surface current response of the scatterer. For thin wire models the surface current can be assumed to flow solely in the direction of the axis of each wire segment. Furthermore, certain approximations can be made which reduce the Green's function integral to a one-dimensional integral along the axes of the wire segments comprising the model.

An equation for the current response can be obtained by applying the surface boundary conditions. The most important of these is that:

(1) the tangential component of the sum of the scattered and incident fields at the surface is linearly proportional to the local surface current.

For perfect conductors the proportionality constant is zero and consequently, the tangential component of the total E-field is zero at the surface. Condition (1) reduces the Green's function integral to an integral equation which relates the induced surface current distribution to the known tangential component of the incident E-field at each point on the surface.

The integral equation can be solved by using the method of moments. This consists of introducing a set of linearly independent basis functions. The TWFD code uses a set of overlapping triangle

functions as discussed in detail in reference [1]. The unknown current $I(\zeta)$ can be expressed as a linear combination of the basis functions $T_i(\zeta)$, e.g.,

$$I(\zeta) = \sum_{i=1}^{M} u_i \, T_i(\zeta) \tag{2}$$

(here ζ is a parameter which specifies position along the wire segments). In practice the number of bases, M, is finite and not complete. Thus, at best the sum in equation (2) provides an approximation to the actual current. Taking the scalar product of each basis with the tangential component of the incident E-field reduces the integral equation to a matrix equation,

$$V = \tilde{Z} \, I \tag{3}$$

where V is an M x 1 vector whose components are these scalar products, I is an M vector whose components are the unknowns u_i, and Z is the M x M impedance matrix.

There are additional boundary conditions which must also be satisfied. These are:

(2) the current at free segment ends must be zero,

(3) the net current flowing into any junction must be zero, and

(4) the charge density ($dI/d\zeta$) for all segments meeting at a junction must converge to the same limit at the junction.

These conditions introduce additional linear constaints on the coefficients u_i which reduce the number of independent variables. This requires the reduction of equation (3) to an M′ dimensional matrix equation where M′< M. The details of this reduction are discussed in reference [1]. In this reduced representation the u_i are linear combinations of the indepenent components of the unknown vector I′, viz,

$$I = B\ I' \tag{4}$$

where B is an M x M′ matrix which contains the boundary conditions. The vector V′ and the M′ x M′ reduced impedance matrix Z′ can be evaluated directly. The surface response can thus be obtained for a given frequency by finding $(\tilde{Z}')^{-1}$, forming

$$I' = (\tilde{Z}')^{-1} V' \quad , \tag{5}$$

and then making use of equation (4).

The scattered cw field can be obtained by integrating the Green's function with the surface current response. Using equation (2) it is straight forward to show that this incegral reduces to a vector product, viz,

$$H\ (\omega,\Omega) = G \cdot I \tag{6}$$

where G is a 1 x M row vector whose components are the scalar products of the Green's function and the basis functions. By forming

$$G' = G\ B \tag{7}$$

it follows that

$$H\ (\omega,\Omega) = G'\ (Z')^{-1}\ V' \tag{8}$$

Equation (8) is the solution of the cw scattering problem. If wire segments have non-zero diameters, the matrix Z′ will be non-singular and, hence, invertible for all real ω.

It is important to note where the Ω dependence is in equation (The vector V′ depends on the incident propagation direction and polar zation. The vector G′ depends on the position of the observation poi as well as the observed polarization. The impedance matrix depends neither on the polarizatons nor the directions of the incident and observed fields. It strictly depends on the scattering system itself However, all three factors on the right side of equation (8) depend o the frequency.

We can make use of analytic continuation to extend equation (8) the ω-plane. The singularity expansion method (SEM) [4] says that we can do this except at certain discrete singularities. It has been sh that

$$H(\omega,\Omega) = -j \sum_{i=1}^{N} \frac{A_i(\Omega)}{\omega-\omega_i} + W(\omega,\Omega) \qquad (9)$$

Equation (9) is equation (1) rewritten using the transformation s=jω. The TWFD code converts the s-plane representation to the equivalent ω-plane representation when doing the calculations.

The singularities are due to the impedance matrix. Both G′ and are analytic everywhere. It follows that the singular points ω_i are roots of $\det(\tilde{Z}')$. The primary function of TWFD is to find these root which are the resonance poles. The method of moments approach shows very clearly that these poles are independent of incident and scatte aspects and polarizations.

The TWFD is also capable of calculating $A_i(\Omega)$ and $H(\omega,\Omega)$ for any combination of the variables Ω. Indeed, parametric studies of Ω can be done quite readily by recognizing that its dependencies are contained within G' and V' which are easily calculated. This will be discussed more thoroughly in the following sections.

3.0 LOCATING THE RESONANCE POLES

The primary function of TWFD is to predict the positions of resonance poles. This is accomplished by finding the zeros of $D(\omega) = \det(Z'(\omega))$. We initially used a technique which applied contour integration to the evaluation of the zeros. This was mentioned in Reference [1]. Unfortunately, this approach required that $D(\omega)$ be evaluated at an unacceptably large number of points. The time requirements were prohibitive. We then resorted to using a steepest descent approach. This has proven to give good results and decreased the calculation time by almost two orders of magnitude. The only concern with using steepest descent is the possibility of missing a pole. However, our numerical tests have shown this fear to be unwarranted, especially since the TWTD code provides an independent means of checking the TWFD results.

The steepest descent technique converges to a zero of $D(\omega)$ starting from an initial guess. This is done as follows. At some initial guess ω_o a "shooting vector" $\Delta\omega_o$ is calculated which leads to a new guess $\omega_1 = \omega_o + \Delta\omega_o$. At ω_1 a "shooting vector" $\Delta\omega_1$ is calculated which leads to another guess. The sequence of guesses converges to a zero. The sequence $|\Delta\omega_n|$ converges monotonically to zero. The position of a pole is sufficiently approximated as ω_n when $|\Delta\omega_{n-1}| < \epsilon$ where ϵ is some small preselected positive number. In practice a half dozen or fewer iterations of this process is usually sufficient. The number n depends on how close the initial guess is to an actual pole.

The basis of the technique is to produce an appropriate "shooting vector" $\Delta\omega_n$ at each successive guess ω_n. This is done by forming $A(\omega_n) = |D(\omega_n)|^2$ and $\text{grad}(A(\omega_n))$. By using the Cauchy-Rieman conditions it is possible to obtain A and its gradient by calculating D at ω_n and $\omega_n + \Delta x$ where Δx is a real-valued differential step. The direction of

the "shooting vector" is that of grad$A(\omega_n)$ and its magnitude is $|A(\omega_n)|/|\text{grad}(A(\omega_n))|$. The code includes another factor which helps speed up the convergence if the initial guess is not close to a pole. However, the technique used is essentially that described.

The frequency plane is generally normalized so that for the lowest order poles $\text{Re}(\omega) \cong 1$. Using $\varepsilon = .001$ we have found that convergence is often achieved with 2 or 3 iterations and almost always within 5 or 6. Since D has to be calculated at two points for each "shooting vector", it follows that for each pole prediction $D(\omega)$ must be calculated at about 4 to 10 points.

Convergence is not always achieved. The criterion we chose for non-convergence is two successively increasing values of $|\Delta\omega_n|$. Our experience with running TWFD has shown that as we increase the order of the pole being sought, non-convergence becomes a problem. The reason for this is that the finite basis set cannot be adequately used to represent the higher modes. If we significantly increase the number of bases, more higher order poles can be found. However, for any particular basis set, we find that there is a maximum pole order to which we can converge. In short the cost per pole increases dramatically with increasing pole frequency. In practice the maximum frequency of interest can be obtained by knowing the spectral response of the transmit/receive system in which we are interested.

4.0. CALCULATING THE RESIDUES

The calculation of the residues $A_i(\Omega)$ (see equations (1) and (9)) is another capability we have built into TWFD. Most particularly we are interested in how they depend on the directions and polarizations (denoted by Ω) of the incident and detected fields. Using the technique outlined in this subsection, parametric studies of this kind can be carried out readily and quite efficiently.

The formulation of the technique can be seen by combining equations (8) and (9). From these we have that

$$A_i(\Omega) = jG'(\omega_i) \quad \tilde{A}'_i \; V'(\omega_i) \tag{10}$$

$$\text{where } \tilde{A}' = \lim_{\omega \to \omega_i} (\omega - \omega_i) \left(\tilde{Z}'(\omega_i)\right)^{-1} \tag{11}$$

In equation (10) we have used the fact that G' and V' are analytic everywhere. All the Ω dependence is contained in these two vectors which are easily calculated. The matrix $\tilde{A}'_i$ associated with each ω_i is independent of Ω. Almost all the computational effort in calculating $A_i(\Omega)$ is in calculating $\tilde{A}'_i$. Thus, what we do is to obtain $\tilde{A}'_i$ once, when we locate ω_i, then store it for later use in doing parametric studies of $A_i(\Omega)$.

The validity of this technique depends on the reliability with which we can numerically form the limit in equation (11). There are various ways of doing this. We have chosen the most straightfoward approach and have found that it gives good results. The approach is as follows. Let a'_i and z'_n be corresponding components of $\tilde{A}'_i$ and $\left(\tilde{Z}'(\omega_n)\right)^{-1}$, respectively. If $|\Delta\omega_{n-1}| < \varepsilon$, we assume

$$a_i' = (\omega_{n-1} - \omega_i)\, z'_{n-1} \tag{12a}$$

$$a_i' = (\omega_n - \omega_i) z'_n \tag{12b}$$

where ω_i is the actual pole which ω_{n-1} and ω_n approximate. The unknown ω_i can be eliminated to obtain

$$a_i' = \frac{\Delta\omega_{n-1}\ z'_{n-1}}{(z'_{n-1}/z'_n)-1} \quad . \tag{13}$$

The value of a_i obtained from equation (13) is actually an approximation which depends on the convergence criterion ε. Our initial numerical tests showed that a_i was weakly dependent on ε in the region of the values which we typically use for this parameter (.01-.0001). This indicated that equation (13) provided a good approximation of a_i'. As ε was given smaller values, random variations in a_i' began to occur because of the inherent numerical inaccuracies of the computer. More extensive tests revealed that there are some poles for which the technique described in equations 12 and 13 does not give an adequate convergence of the limiting process of equation (11). This is discussed in section 6.3. At this point it is not clear to us why the technique should work well for some poles and not work for others. We intend to resolve this problem in a future study.

5.0 PREDICT THE IMPULSE RESPONSE

The impulse response can be obtained by applying equation (8) to points on the real-ω axis. In practice we perform this calculation at a discrete and finite set $\{\omega_\ell | \ell=1,M\}$ of such points. A DFT applied to this set then provides a prediction of the impulse response for a discrete set $\{t_m | m=1,M\}$ of sampled points in the time domain.

It is desirable that the time t_1 correspond to the initial reception of the scattered signal at the receiver. The impulse response obtained from equation (8) will be referenced to the time at which the incident impulse crosses the origin of the coordinate system. Let t' be the time referenced to this latter event. Let t be the time referenced to the initial reception of the response. It is necessary to determine τ so that t' and $\tau + t$ correspond to simultaneous points in time. The desired transfer function then becomes

$$H_1(\omega,\Omega) = e^{-j\omega\tau} \; H(\omega,\Omega), \tag{14}$$

and the corresponding impulse response will be referenced to time t with $t=0$ corresponding to the first sample point t_1.

For the far-field response τ can be determined quite readily. Let

$$\tau = \tau_o - \Delta\tau \tag{15}$$

Where τ_o corresponds to the time it takes for a signal to travel from the origin to the observation point. In the calculations the origin is always chosen as a point on the target. Because of the target's finite size it is possible for scattering from some of its points to reach the receiver before the initial reception of scattering from the origin. The time $\Delta\tau$ accounts for this effect. Figure 1 illustrates the difference between the times τ_o and τ.

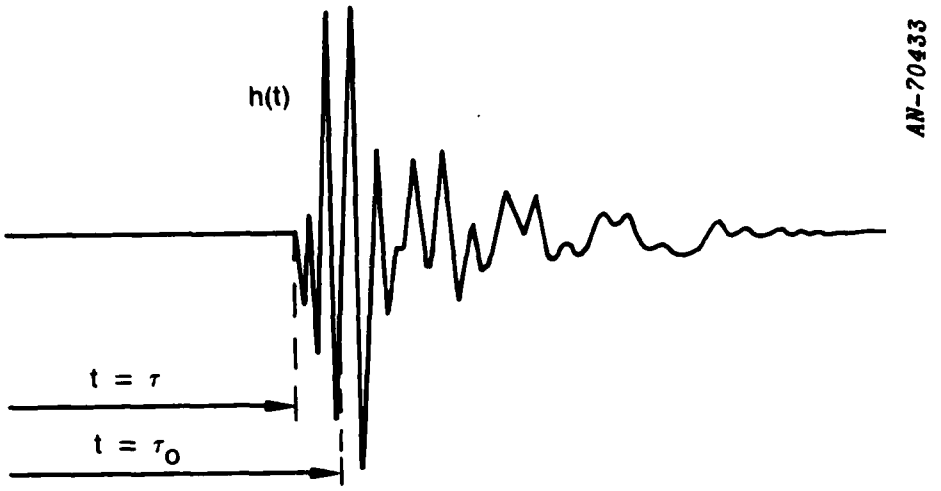

Figure 1 Far Field Impulse Response, h(t), of a target. The original of the coordinate system is chosen as a point on the target. The time τ is the earliest that scattering from the origin can reach the receiver. Because the target has a finite size the initial reception of target scattering can occur at some time $\tau < \tau_0$.

The time τ_o is readily determined from the distance between the observation point and the origin. It turns out that the factor $e^{j\omega\tau_o}$ appears explicitly in G' of equation (8). Thus, by simply omitting it in the calculation, the translation to time τ_o is made. Doing this it follows that

$$H_1(\omega,\Omega) = e^{j\omega\Delta\tau} H(\omega,\Omega) \quad . \tag{16}$$

Equation (A.1) is the explicit form of $H(\omega,\Omega)$ for a thin wire scatterer. The time $\Delta\tau$ is determined from the unit directional vectors $\hat{n}$ and $\hat{m}$ which point, respectively, from the origin to the transmitter and receiver. Let $\vec{r}$ represent the position of any point on the scatterer relative to the origin. It is easy to show that

$$\Delta\tau = \underline{\text{Max}}\left(\frac{\vec{r}\cdot(\hat{n}+\hat{m})}{c}\right) \quad . \tag{17}$$

The receiver will act as a filter on the signal. This can be represented by some transfer function $F(\omega)$ which can be included in the calculations. A prediction of the measured transient response is then obtained by applying a DFT to

$$H_2(\omega,\Omega) = F(\omega)\cdot H_1(\omega,\Omega) \quad . \tag{18}$$

The function $F(\omega)$ provides a natural cutoff for the maximum frequency needed.

6.0 NUMERICAL RESULTS AND VALIDATION

This section presents the results of the TWFD validation study. In all cases TWFD numerical results were validated with TWTD numerical data or experimental measurements or both. All of the aspects of TWFD were studied and tested. These studies include:

1. Pole estimated from zeros of impedance matrix (Section 6.1)

2. Prediction of scattering cross section and impulse response (Section 6.2)

3. Production of scattered field polar residue patterns (Section 6.3)

The results for studies 1 and 2 validate TWFD quite well. The results for study 3 pointed out a numerical convergence problem when we attempted to perform the limiting process of equation (11).

Two canonical (analytically predictable) stick aircraft were modeled using TWFD for the series of validation tests. These models are shown schematically in Figure 2. The two targets were chosen so that both TWFD and TWTD could be used and so that the experimental targets could be constructed easily in varying scales. The modified stick model differs from the standard stick only in the location of the horizontal stabilizer. The choice of the simple target shapes allows for a first order correlation of the resonances with the target configuration.

This section only displays the results of the validation tests. These data presented here along with more extensive results were used in a companion ONR study investigating the use of resonance extraction for target identification and characterization. That study is summarized in a three-volume final report [5].

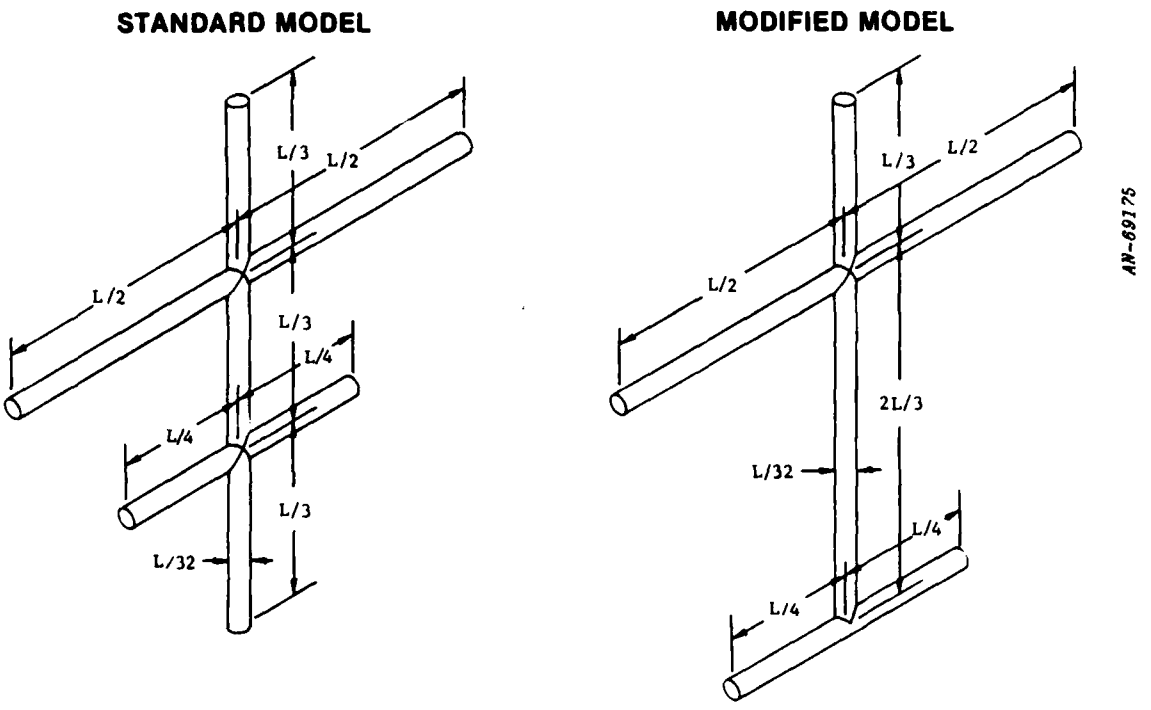

Figure 2 Comparison of the two canonical stick model targets used to validate TWFD with TWTD and the measured data.

6.1 POLE ESTIMATES

An initial check on the resonances produced using TWFD was in fact a self check. GRC's Prony's method algorithm [1,5] was applied to the scattered fields produced by TWFD. The resulting extracted poles are compared to the poles obtained from zeros of the determinant of the TWFD impedance matrix in Table 1. As would be expected, the poles produced by the two mechanisms are very close. Table 1 also shows the aspect angle independence of the resonances of the two stick models.

In order to properly validate the poles produced from the TWFD impedance matrix, resonances were extracted from measured fields. These fields were measured in a cw scattering chamber (described in detail in reference [5].) Tables 2 and 3 compare the extracted poles at each of the nine scattering angles with the theoretically produced TWFD poles. Figures 3 and 4 plot the poles of Tables 2 and 3 respectively in the complex s plane. These figures graphically show the clustering of the poles as a function of angle and any deviation of the cluster mean from the theoretically predicted value.

The results of these pole extraction studies convinced us that the code was working within numerical expectations. Hence TWFD can be used as an independent validation tool for resonance extraction tests.

6.2 SCATTERED FIELDS

The scattered fields predicted by TWFD for the two canonical targets were compared to three other data sources in both the time and frequency domain. The TWTD numerical model was used to produce smoothed impulse responses directly in the time domain. Spectral data was obtained by performing a FFT on the data. The scattering spectrum was measured directly in the frequency domain using a cw measurement system

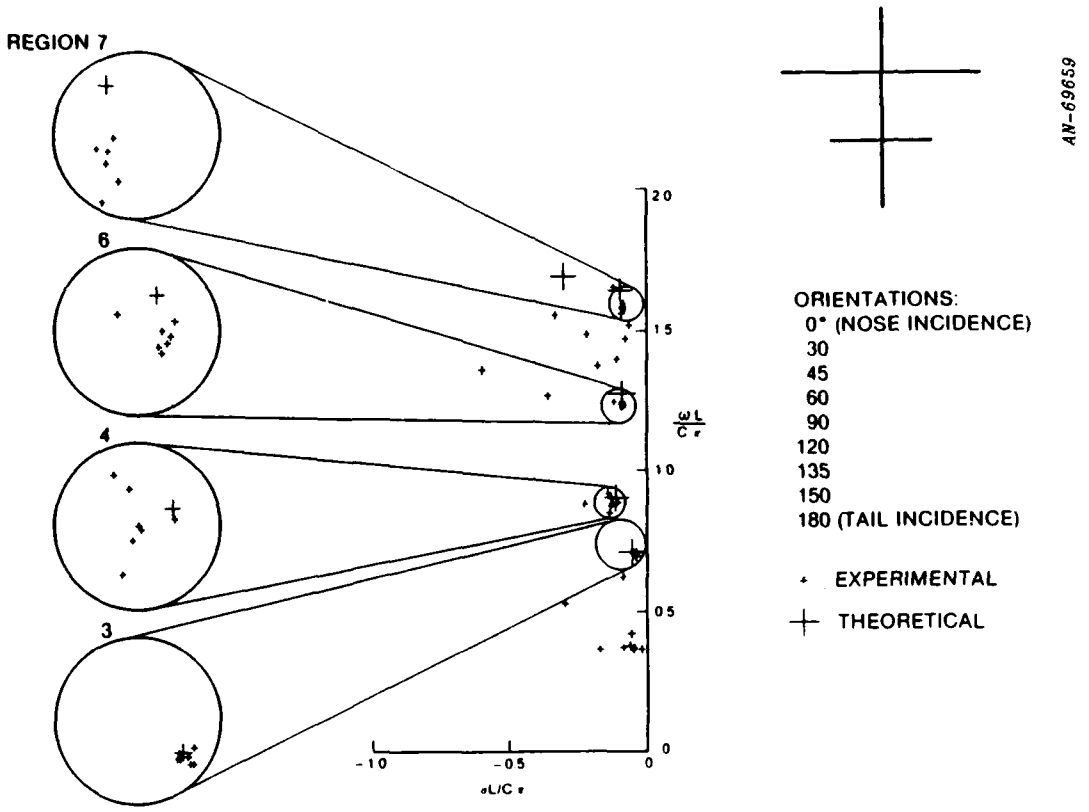

Figure 3 Overlays of poles estimated from cw measured responses (Table 2) at all orientations for standard stick model. The theoretical values are shown with the large +.

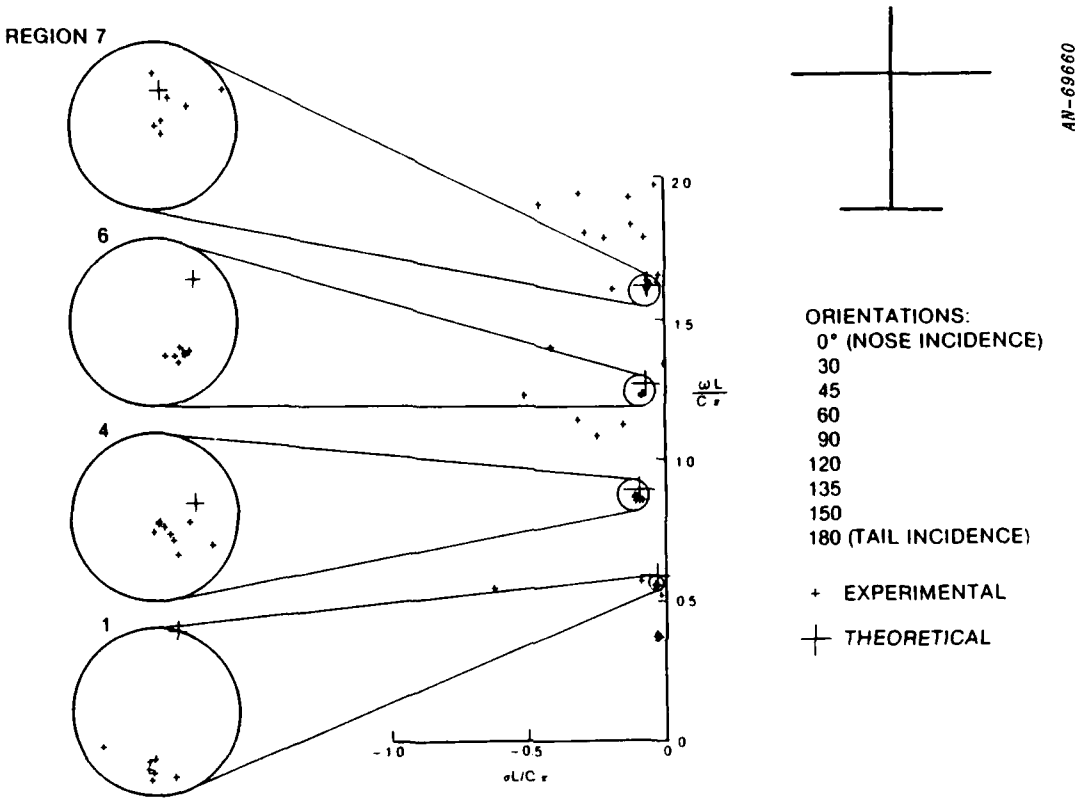

Figure 4 Overlays of poles estimated from cw measured responses (Table 3) at all orientations for the modified stick model to the TWFD produced theoretical poles shown with a large +.

Table 1 Comparison of poles estimated by applying Prony's method t noise-free numerical responses to theoretical values obtai from zeros of the TWFD impedance matrix determinant for th standard and modified stick models.

	STANDARD STICK				MODIFIED STICK			
ANGLE(DEG)	POLE 1	POLE 2	POLE 3	POLE 4	POLE 1	POLE 2	POLE 3	POLE
0.	-----	-0.110	-----	-----	-----	-0.106	-----	-----
30.	-0.047	-0.111	-0.083	-0.084	-0.039	-0.106	-0.080	-0.0(
45.	-0.047	-0.110	-0.083	-0.087	-0.039	-0.105	-0.080	-0.0(
60.	-0.047	-0.110	-0.083	-0.087	-0.039	-0.106	-0.080	-0.0(
90.	-0.047	-----	-0.083	-0.087	-0.039	-----	-0.080	-0.0(
120.	-0.047	-0.110	-0.083	-0.087	-0.039	-0.106	-0.080	-0.0(
135.	-0.047	-0.110	-0.083	-0.087	-0.039	-0.106	-0.080	-0.0(
150.	-0.047	-0.110	-0.083	-0.087	-0.039	-0.106	-0.080	-0.0(
180.	-----	-0.110	-----	-----	-----	-0.106	-----	-----
MEAN:	-0.047	-0.110	-0.083	-0.086	-0.039	-0.106	-0.080	-0.0(
THEORETICAL:	-0.044	-0.106	-0.085	-0.084	-0.037	-0.103	-0.076	-0.0(
0.	-----	0.889	-----	-----	-----	0.888	-----	-----
30.	0.705	0.888	1.261	1.627	0.583	0.888	1.264	1.62
45.	0.706	0.889	1.262	1.627	0.583	0.888	1.264	1.62
60.	0.706	0.889	1.262	1.627	0.583	0.887	1.264	1.62
90.	0.706	-----	1.261	1.627	0.583	-----	1.264	1.62
120.	0.706	0.889	1.261	1.627	0.583	0.888	1.264	1.62
135.	0.706	0.889	1.262	1.627	0.583	0.888	1.264	1.62
150.	0.706	0.889	1.261	1.627	0.583	0.887	1.264	1.62
180.	-----	0.889	-----	-----	-----	0.888	-----	-----
MEAN:	0.706	0.889	1.261	1.627	0.583	0.888	1.264	1.62
THEORETICAL:	0.707	0.896	1.266	1.631	0.583	0.893	1.270	1.62

Table 2 Theoretical poles from TWFD compared to the poles estimated from cw measurements at each orientation, their means and standard deviations (error radii) for the standard model).

	REAL PART				IMAGINARY PART			
ANGLE(DEG)	POLE 1	POLE 2	POLE 3	POLE 4	POLE 1	POLE 2	POLE 3	POLE 4
0.	-----	-0.128	-----	-----	-----	0.875	-----	-----
30.	-0.032	-0.104	-0.078	-----	0.714	0.888	1.244	-----
45.	-0.047	-0.129	-0.084	-0.082	0.708	0.908	1.235	1.602
60.	-0.050	-0.134	-0.134	-0.085	0.702	0.852	1.240	1.588
90.	-0.046	-----	-0.085	-0.079	0.702	-----	1.238	1.578
120.	-0.039	-----	-0.083	-0.091	0.704	-----	1.247	1.596
135.	-0.032	-0.138	-----	-0.084	0.696	0.918	-----	1.595
150.	-0.036	-0.124	-----	-----	0.696	0.884	-----	-----
180.	-----	-0.122	-----	-----	-----	0.882	-----	-----
MEAN:	-0.040	-0.126	-0.082	-0.084	0.703	0.887	1.241	1.592
THEORETICAL:	-0.044	-0.106	-0.085	-0.084	0.707	0.896	1.266	1.631
			STANDARD DEVIATION		0.010	0.024	0.006	0.010

Table 3 Theoretical poles from TWFD compared to the poles estimated from cw measurements at each orientation, their means and standard deviations (error radii) for the standard model.

	REAL PART				IMAGINARY PART			
ANGLE(DEG)	POLE 1	POLE 2	POLE 3	POLE 4	POLE 1	POLE 2	POLE 3	POLE 4
0.	-----	-0.117	-----	-0.029	-----	0.872	-----	1.623
30.	-0.037	-0.126	-0.091	-0.068	0.567	0.873	1.228	1.632
45.	-0.040	-0.122	-0.084	-0.060	0.569	0.878	1.224	1.618
60.	-0.040	-0.105	-0.080	-0.067	0.568	0.880	1.229	1.603
90.	-0.039	-0.093	-.078	-----	0.569	0.864	1.230	-----
120.	-0.040	-0.113	-0.079	-0.049	0.568	0.858	1.228	1.614
135.	-0.040	-0.115	-0.083	-0.065	0.567	0.867	1.232	1.606
150.	-----	-0.120	-0.086	-0.064	-----	0.877	1.228	1.599
180.	-----	-0.122	-----	-----	-----	0.880	-----	-----
MEAN:	-0.039	-0.115	-0.083	-0.057	0.568	0.872	1.228	1.614
THEORETICAL:	-0.037	-0.103	-0.076	-0.066	0.583	0.893	1.270	1.621
			STANDARD DEVIATION		0.001	0.013	0.005	0.019

[5]. The impulse response was measured directly in the time domain using a transient scatterig facility [5]. Impulse response and spectral data were obtained from the measured cw and time domain data respectively by using a Fourier transform.

Table 4 is a guide to the TWFD comparisons (Figures 5-15) with the data produced by the three other data sources. All plots showing TWFD smoothed impulse response data are a result of Fourier transforming the spectral data.

A study of Figures 5-15 shows that TWFD data is validated extremely well by the cw measured data. There are minor discrepancies between TWFD and TWTD and between TWFD and the measured time-domain data. In both of these cases the discrepancies can be accounted for my numerical deficiencies n TWTD or noise in the transiet measurements respectively.

6.3 RESIDUE PLOTS

Section 4.0 describes the numerical process used for calculating the angular dependence of the residues associated with each resonance. Figure 16 displays the polar residue magnitude radiation pattern for the first four resonances for the two canonical targets. Figure 17 displays the polar residue plots obtained by applying Prony's method to the TWFD scattered fields at nine discrete angles. By comparing Figures 16 and 17 it is clear that the record residues for each canonical shape do not compare. While the polar plots of Figure 17 are coarse they are felt to be the more accurate. Hence, at the second mode the residue calculation as described in Section 4.0 does not work.

Numerical studies showed that the limiting process does not converge for this particular mode. This may be due to the fact that the second mode is very low Q. At present two methods are available to

correct this problem. However since the production of polar residue plots was not a requirement for TWFD under this work we elected to postpone correcting the residue calculations.

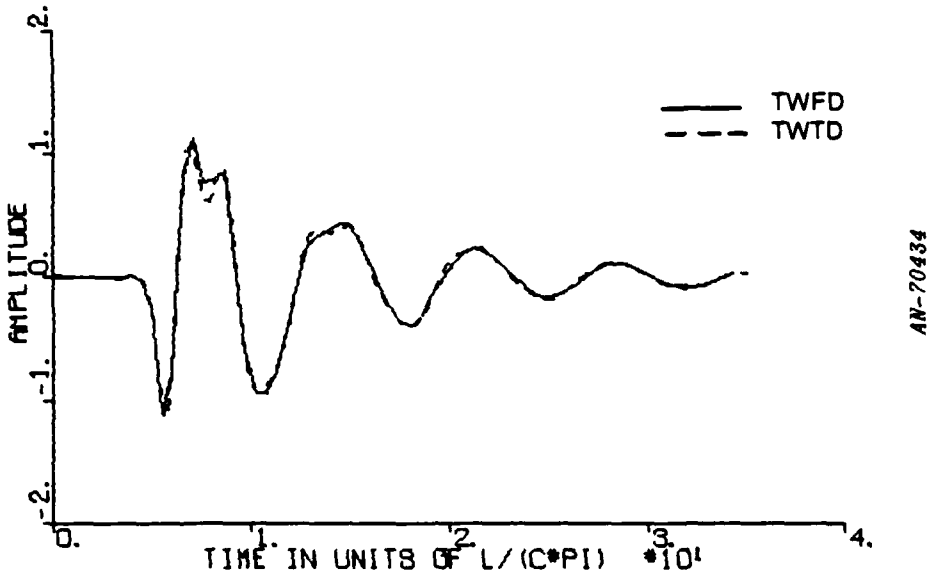

(A)

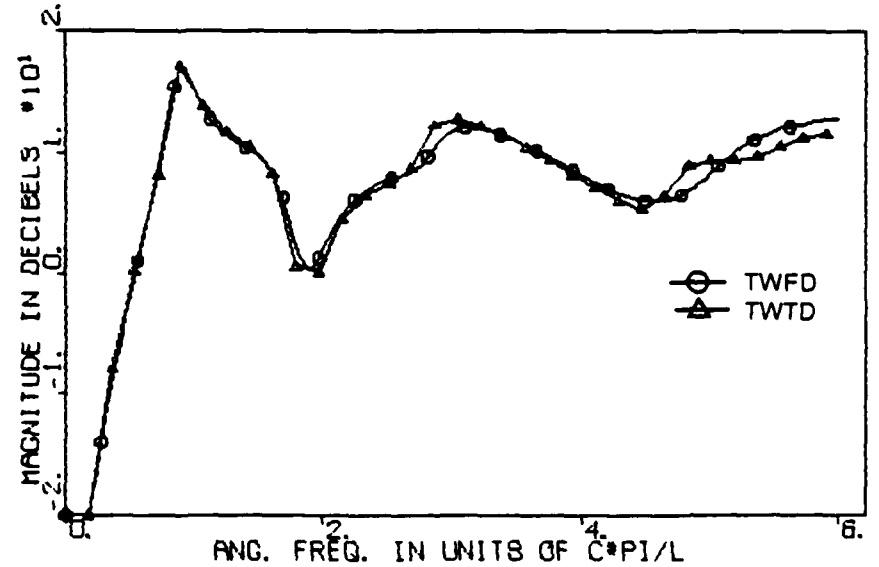

(B)

Figure 5 Comparison of monostatic smoothed impulse response (A), and spectrum (B), of standard stick model at 0° produced by TWTD and TWFD numerical models.

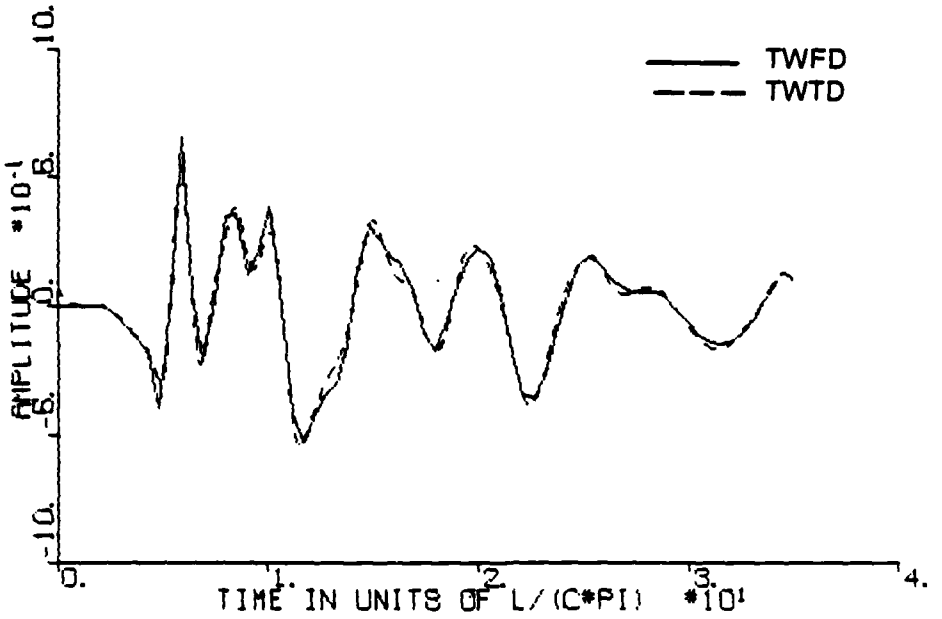

AN-70435

(A)

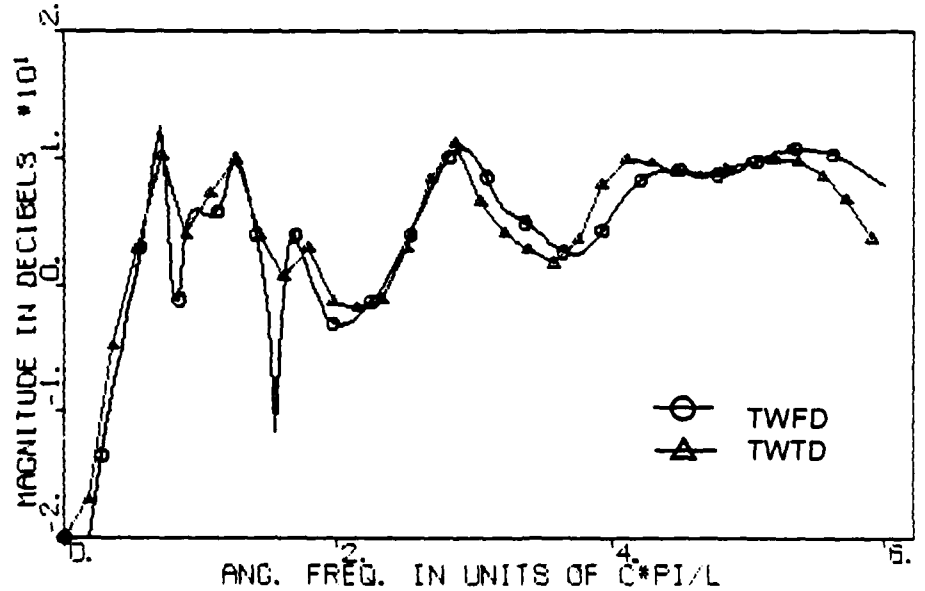

(B)

Figure 6 Comparison of monostatic smoothed impulse response (A), and spectrum (B) of standard stick model at 45° produced by TWTD and TWFD numerical models.

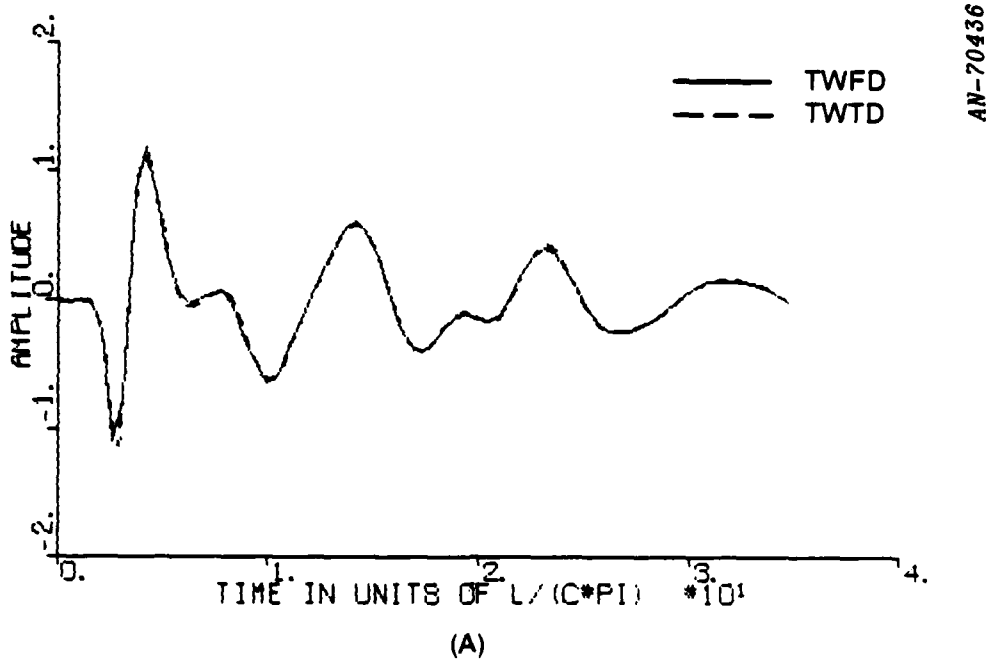

(A)

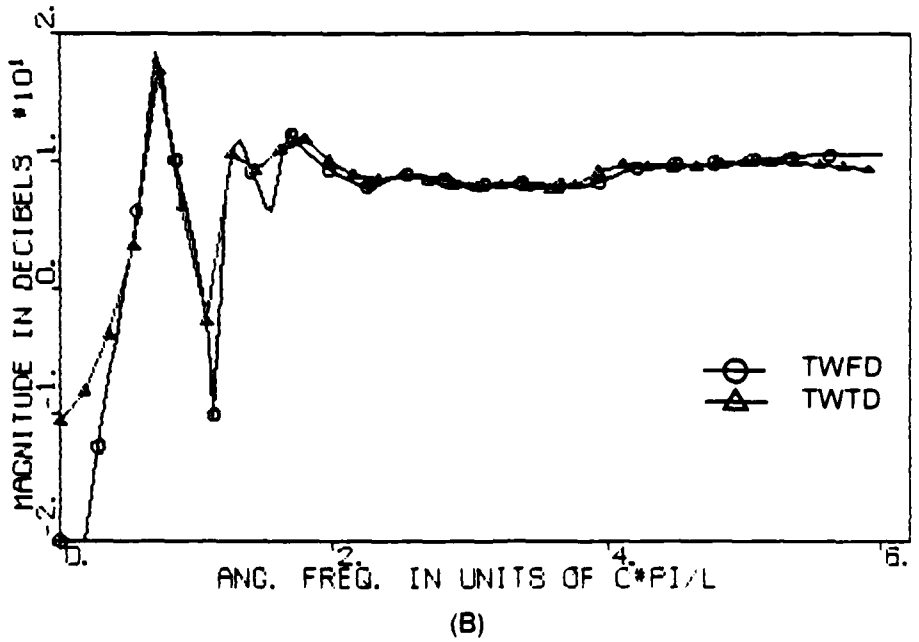

(B)

Figure 7 Comparison of monostatic smoothed impulse response (A), and spectrum (B) of standard stick model at 90° produced by TWTD and TWFD numerical models.

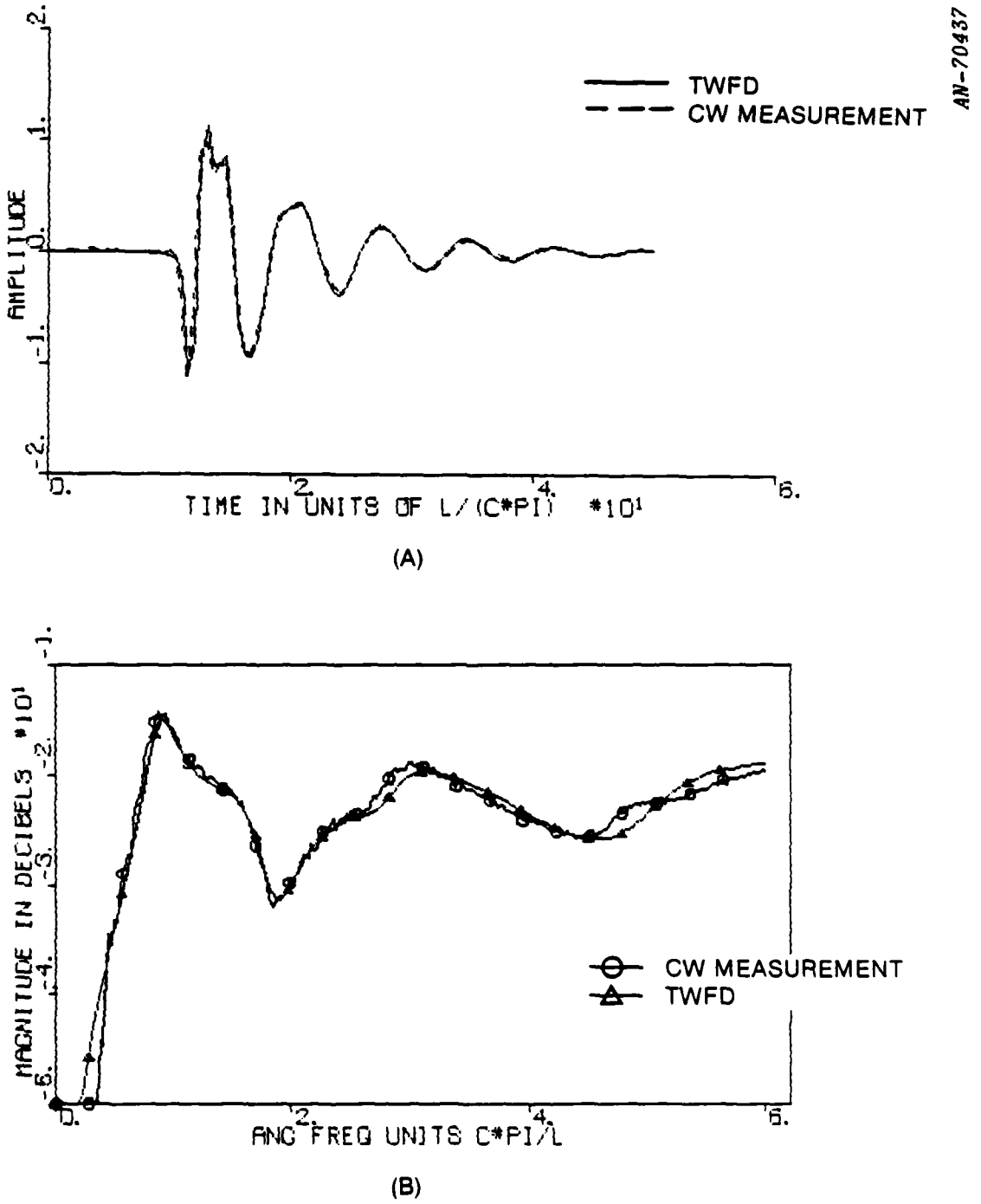

Figure 8 Comparison of TWFD fields to cw measured data at 0° for smoothed impulse response (A) and spectrum (B).

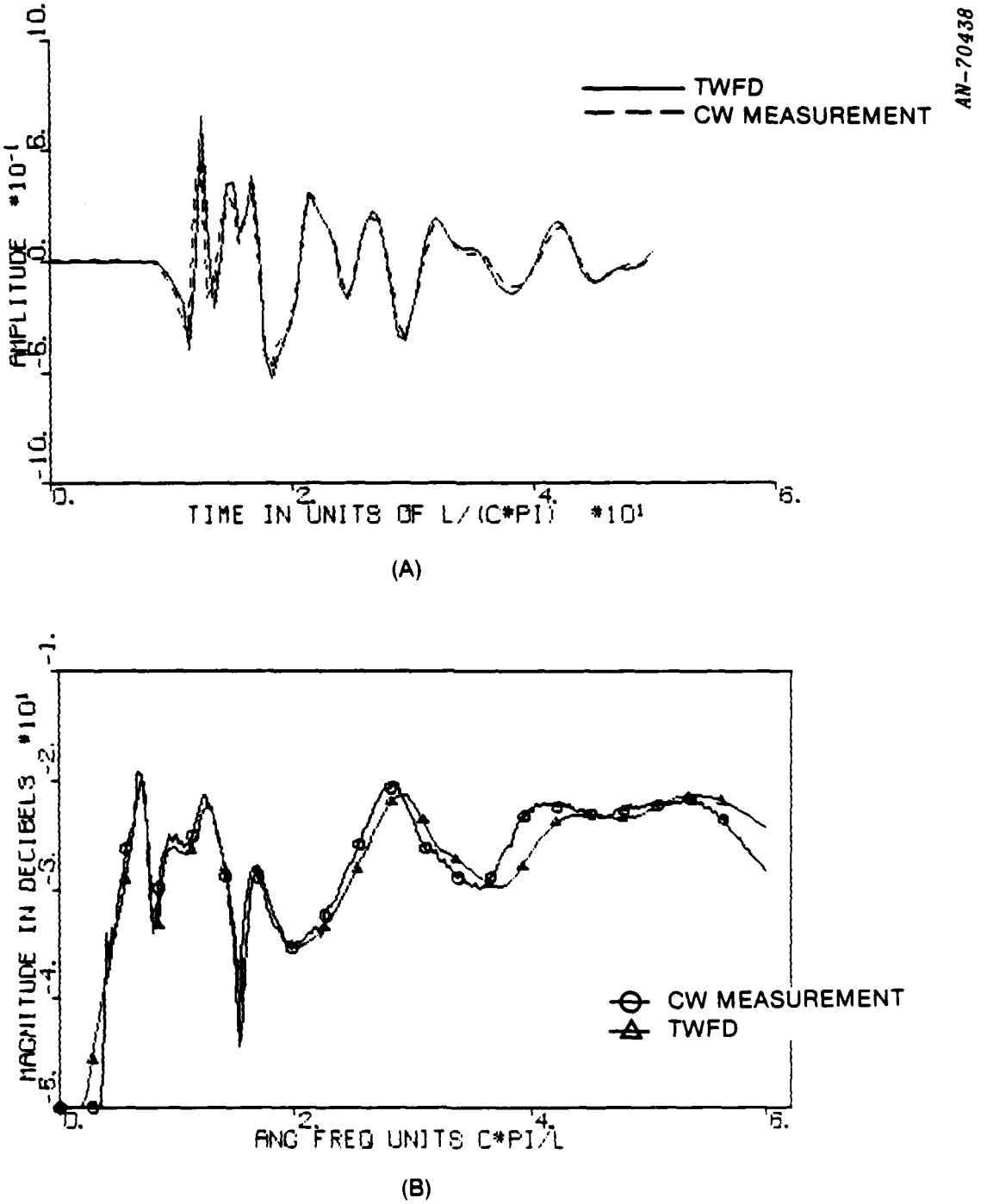

Figure 9 Comparison of TWFD fields to cw measured data at 45° for smoothed impulse response (A), and spectrum (B).

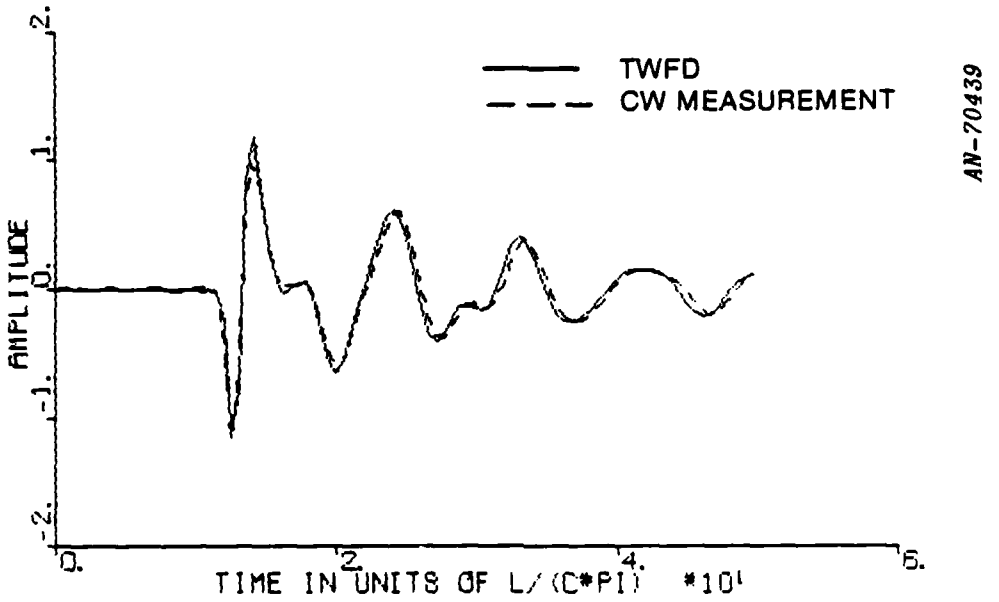

(A)

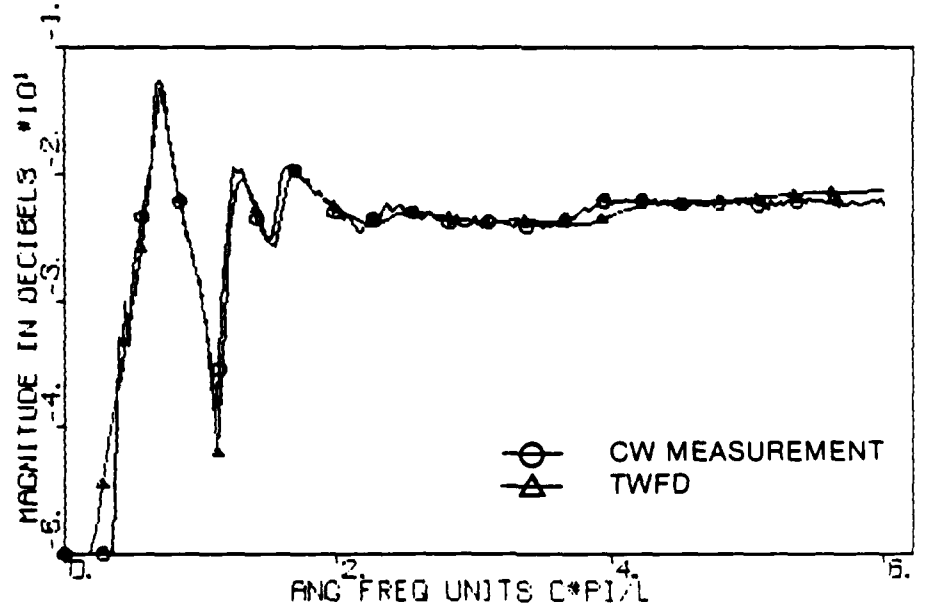

(B)

Figure 10 Comparison of TWFD fields to cw measured data at 90° for smoothed impulse response (A) and spectrum (B).

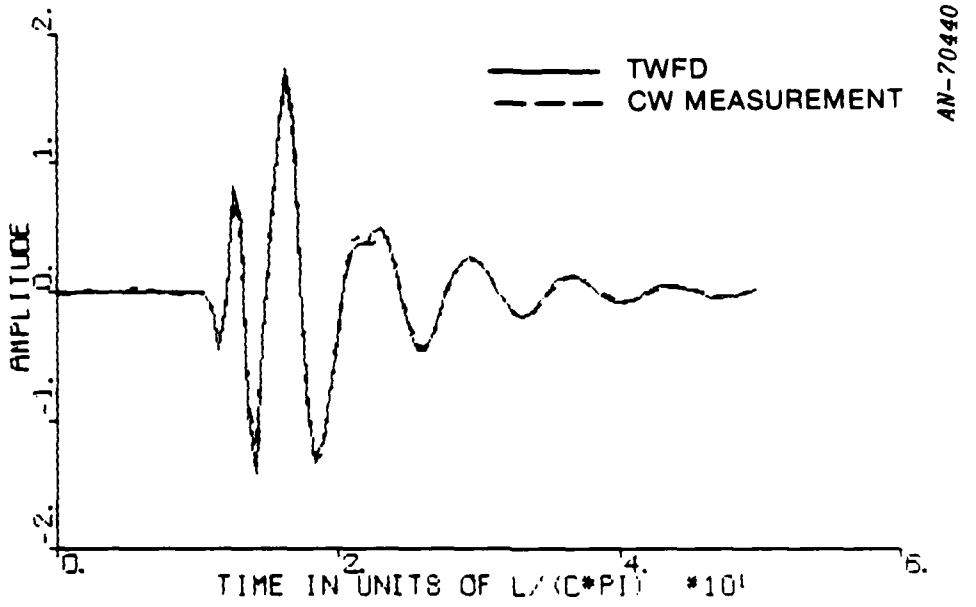

(A)

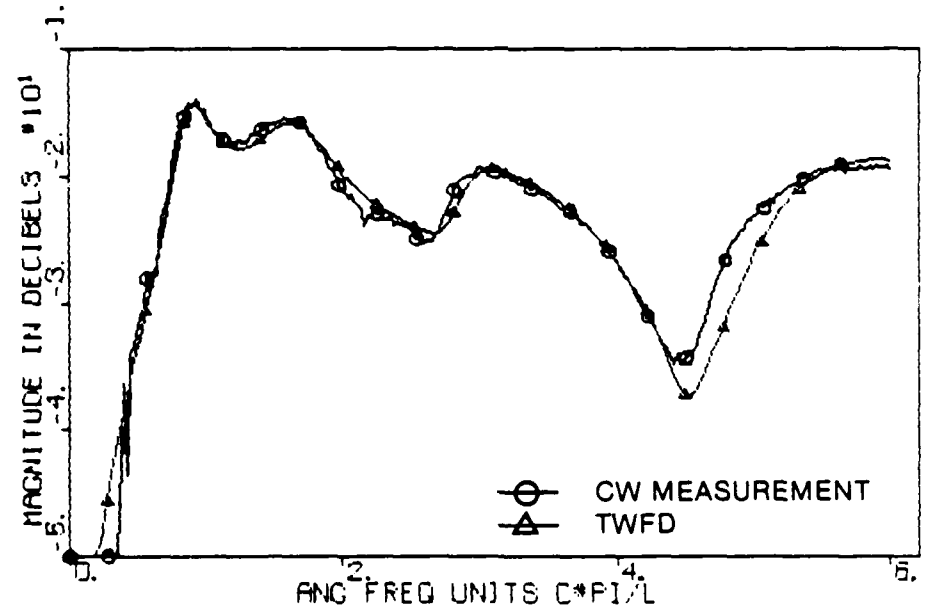

(B)

Figure 11 Comparison of TWFD fields to cw measured data at 180° for smoothed impulse response (A) and spectrum (B).

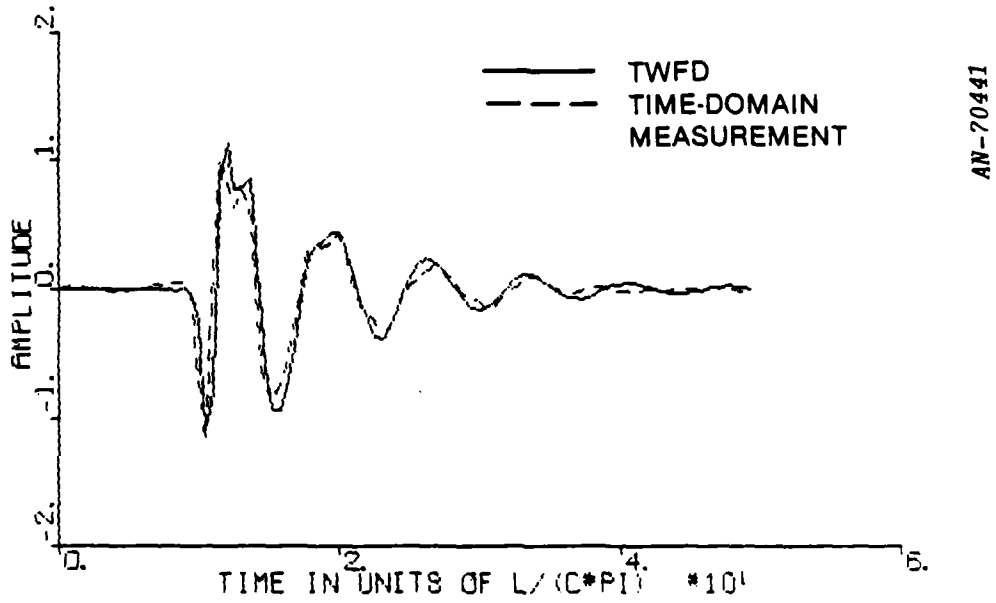

(A)

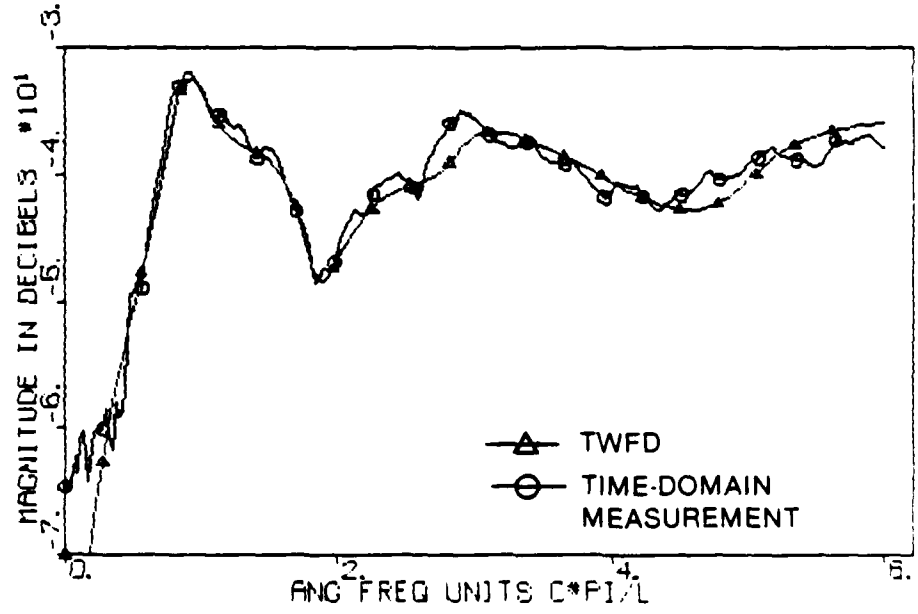

(B)

Figure 12 Comparison of TWFD fields to time-domain measured data at 0° for smoothed impulse response (A) and spectrum (B).

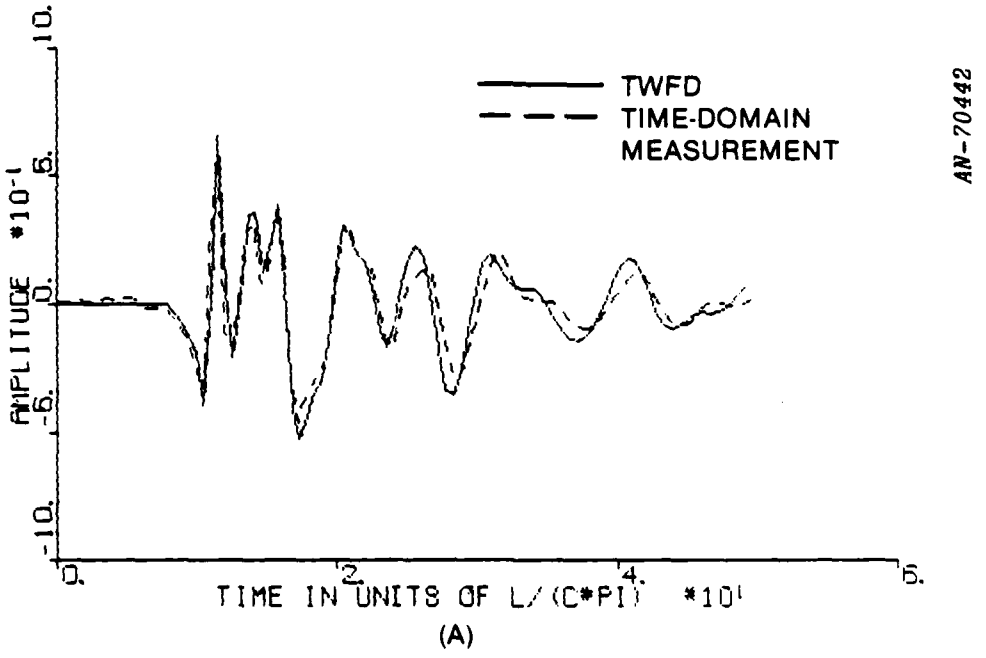

(A)

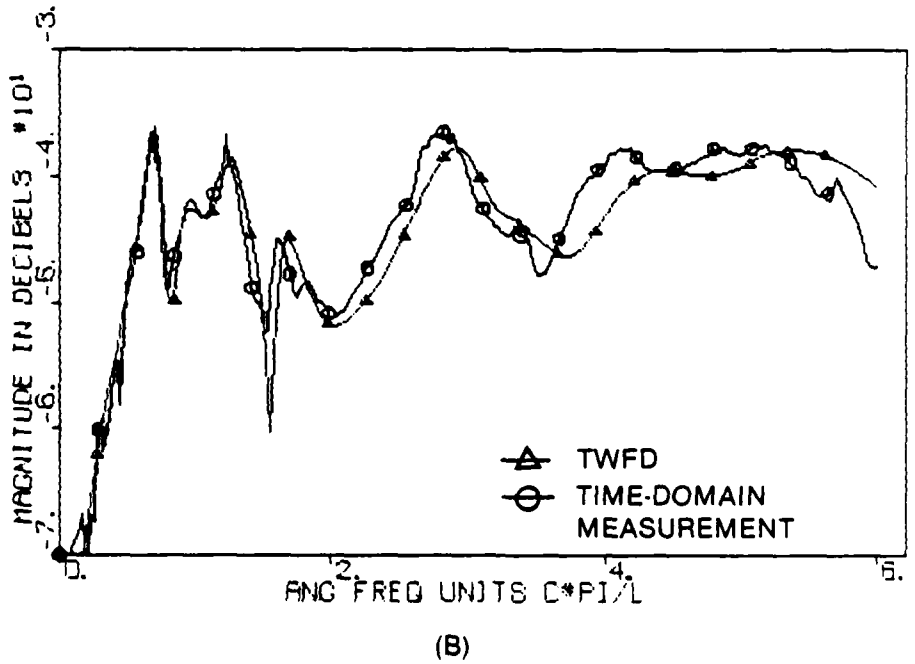

(B)

Figure 13 Comparison of TWFD fields to time-domain measured data at 45° for smoothed impulse response (A) and spectrum (B).

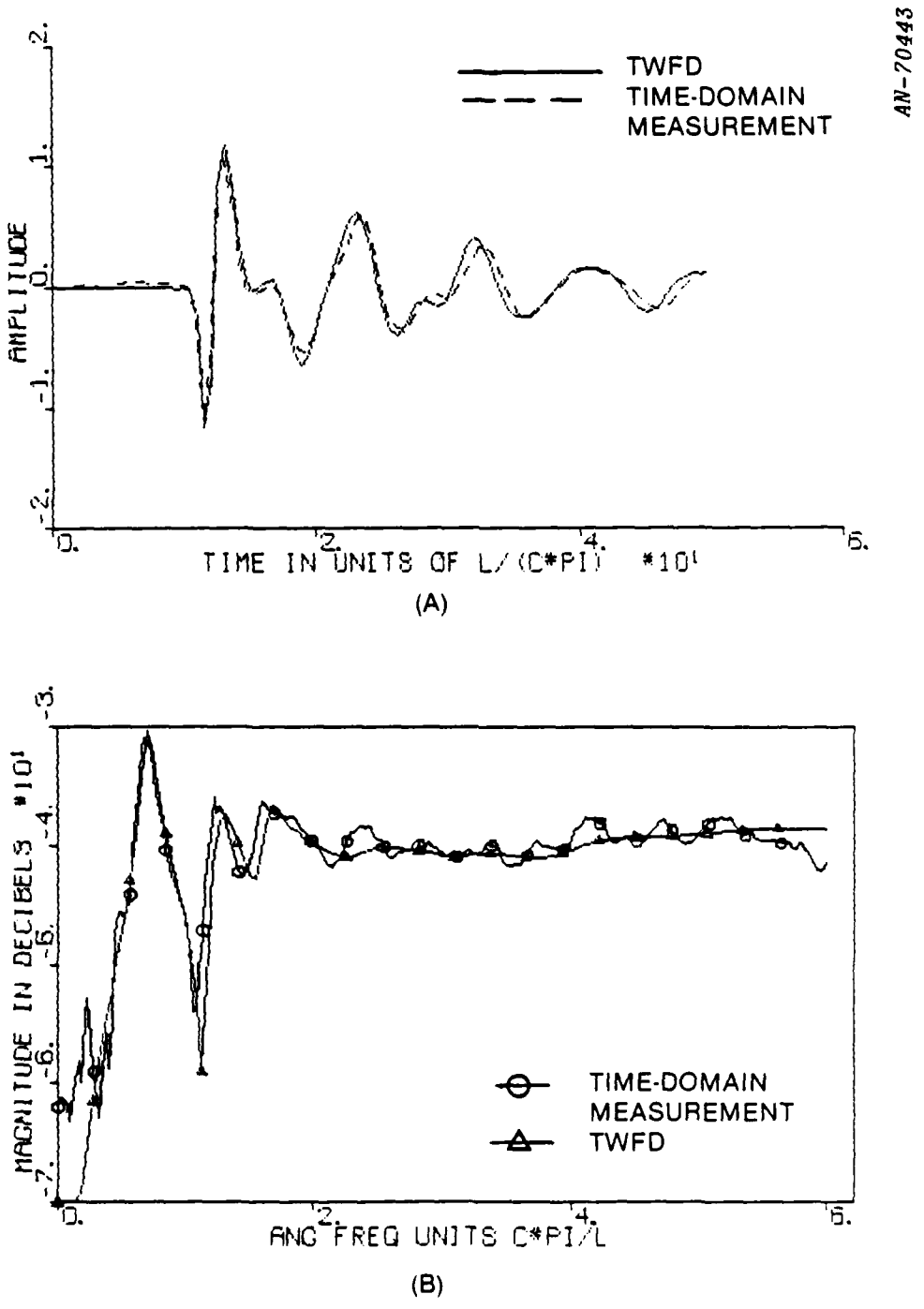

Figure 14 Comparison of TWFD fields to time-domain measured data at 90° for smoothed impulse response (A) and spectrum (B).

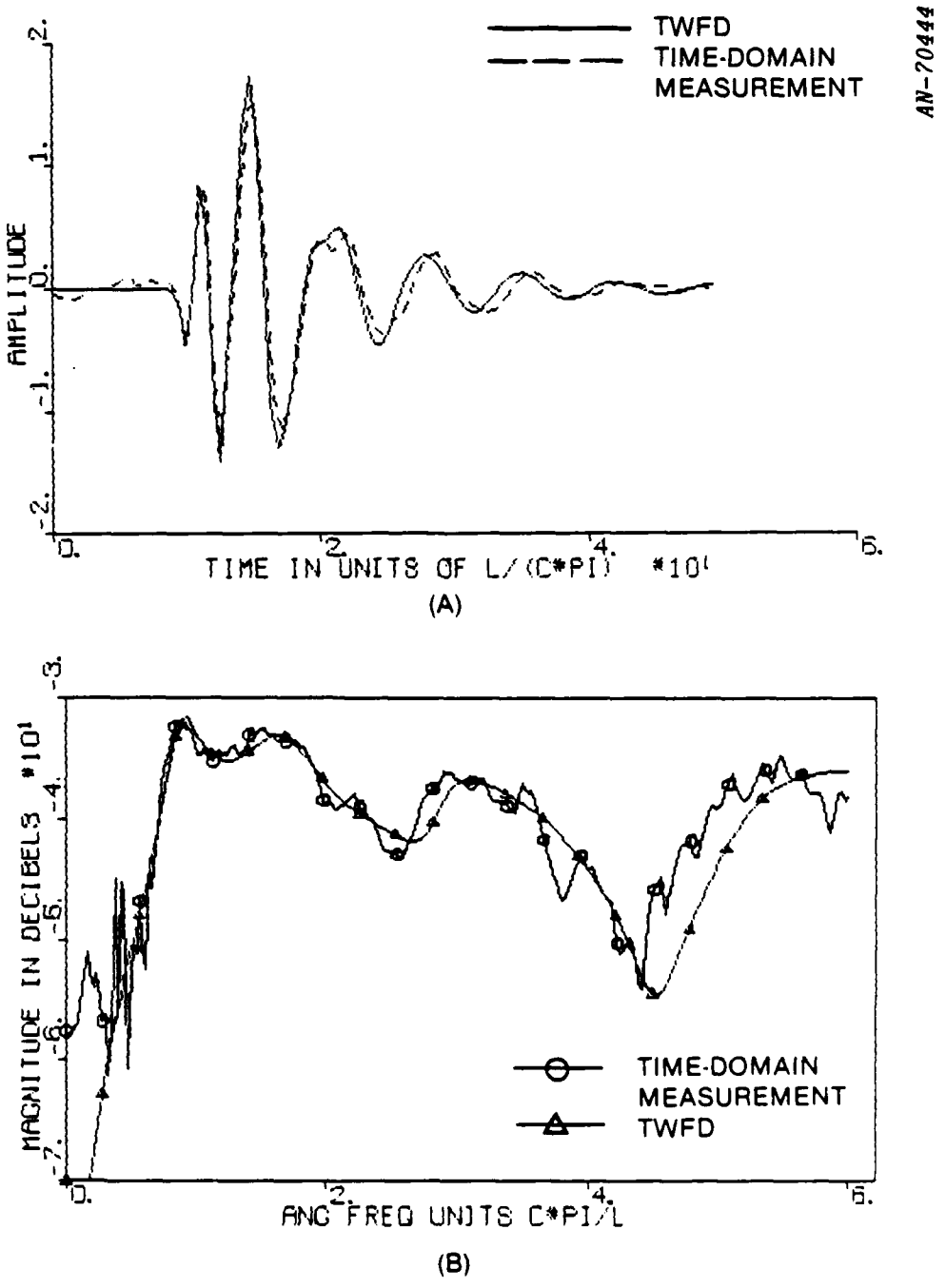

Figure 15 Comparison of TWFD fields to time-domain measured data at 90° for smoothed impulse response (A) and spectrum (B).

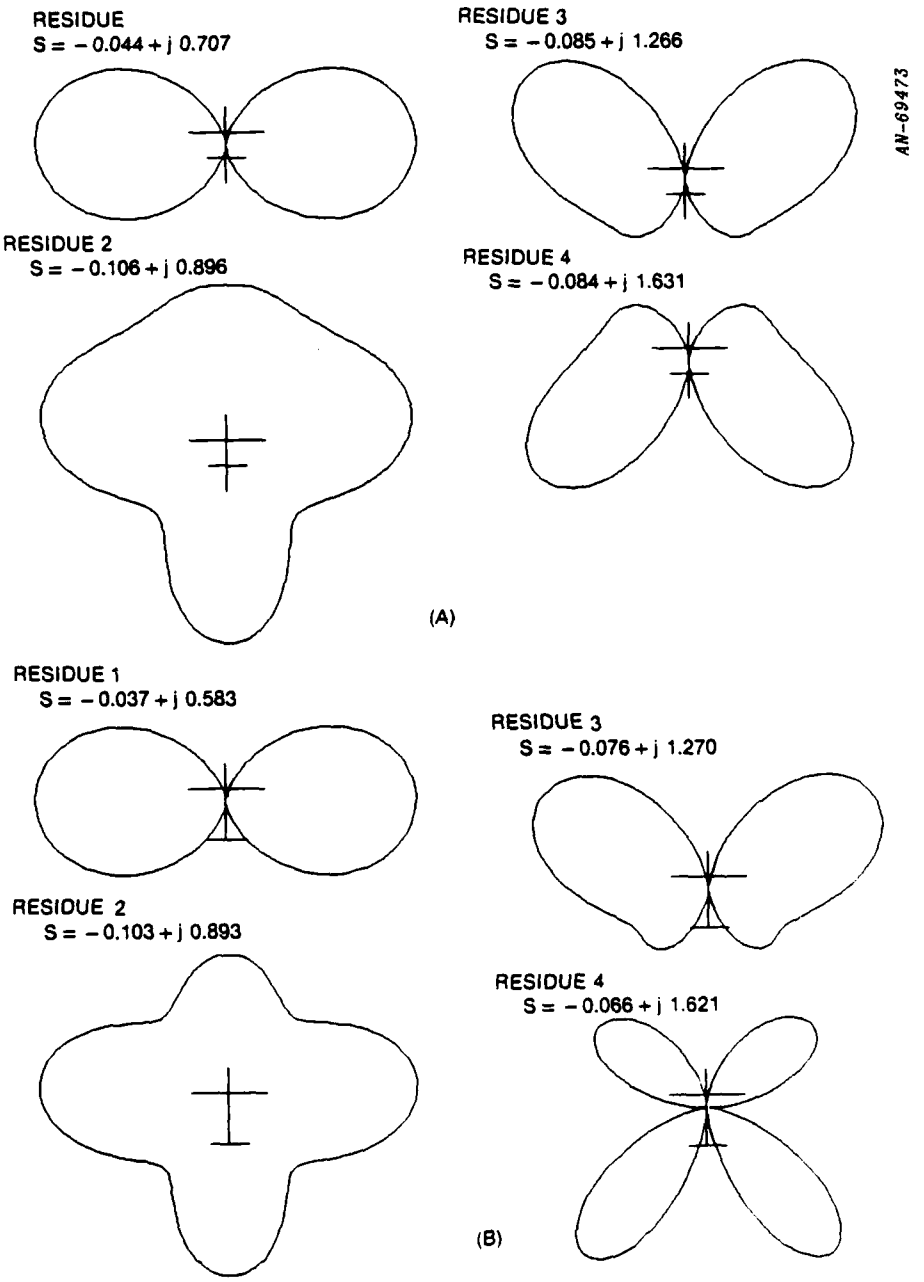

Figure 16 Polar residue magnitude radiation patterns for (A) standard, and (B) modified models. The residues were obtained directly from TWFD as described in the text. It can be shown, by comparison with Figure 17, that due to convergence problems the residues of pole 2 are in error.

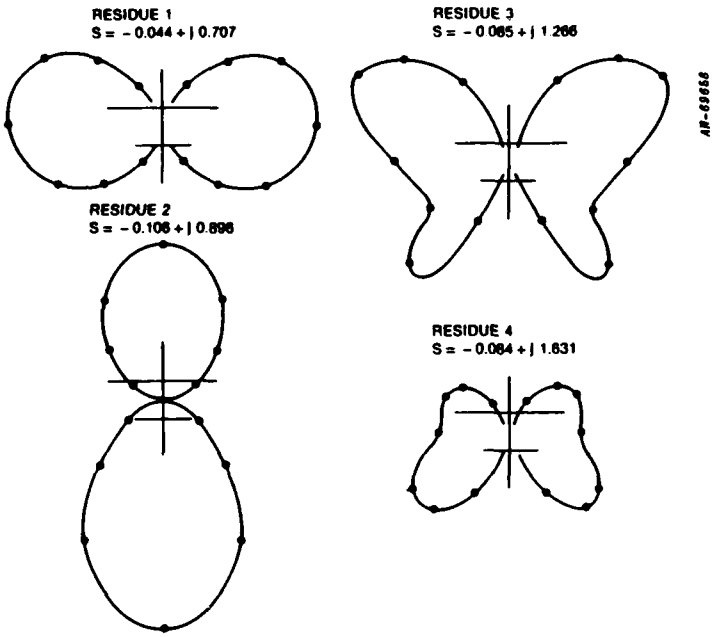

(A)

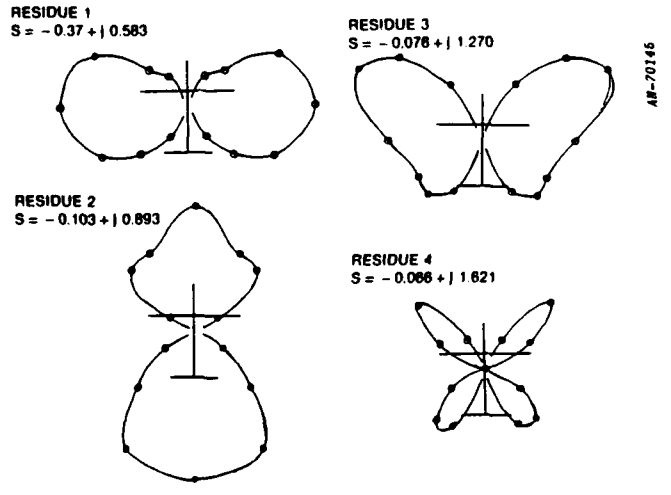

(B)

Figure 17 Polar residue magnitude radiation patterns for (A) standard and (B) modified models. The dots indicate the angles at which the residues were extracted. The curves are manually interpolated from residues extracted from TWFD RCS data by using Prony's method.

Table 4 Guide to the TWFD data comparisons with data produced by three other methods. The Numbers refer to figures in the text.

TWFD	TWTD		MEASURED CW		MEASURED TIME-DOMAIN	
ANGLE	IMPULSE	SPECTRUM	IMPULSE	SPECTRUM	IMPULSE	SPECTRUM
0	5A	5B	8A	8B	12A	12B
45	6A	6B	9A	9B	13A	13B
90	7A	7B	10A	10B	14A	14B
180			11A	11B	15A	15B

REFERENCES

1. J. C. Auton, et. al., "Target Identification and Characterization Using Natural Resonances: Phase 2 Final Report". CR-83-1149, Effects Technology, Inc., (GRC), 15 March 1983.

2. F. M. Tesche, "On the Singularity Expansion Method as Applied to Electromagnetic Scattering from Thin Wires, IEEE Trans AP-21, 53, 1973.

3. M. L. VanBlaricum, "A Numerical Technique for the Time-Dependent Solution of Thin-Wire Structure with Multiple Junctions," Electromagnetic Laboratory Report 73-15, University of Illinois, Urbana, Illinois, Dec. 1973.

4. C. E. Baum, "Transient Electromagnetic Fields" in Topics in Applied Physics, L. B. Felsen, editor. Springer-Verlag, New York 1976.

5. J. C. Auton, T. L. Larry, M. L. VanBlaricum, "Radar Target Identification Using Natural Resonance Extraction". CR-84-1309,1310,1311, General Research Corporation, October 1984.

APPENDIX

This appendix summarizes the details of the calculations represented by equations (8), and (10). The matrices $(Z'(\omega))^{-1}$ and $\tilde{A}_i$ are obtained from the reduced impedance matrix the details of which are described in reference [1].

For electromagnetic scattering from a thin wire structure, the far-field transfer function (normalized to a one meter distance) can be written as:

$$H(\omega,\Omega) = -j\, Z_o\, k_p \int I(\vec{x},\omega,\Omega)\, (\hat{\ell}(\vec{x})\cdot\epsilon)\, \exp\left(jk_p \frac{\hat{n}\cdot\vec{x}}{L}\right)\frac{d\zeta}{L} \qquad (A.1)$$

where $k_p = \frac{\omega L}{c}$

L = length scale factor

Z_o = free space impedance

$\vec{x}$ = position of a point on scatterer

$\hat{\ell}$ = unit directional vector of wire segment

$\hat{\epsilon}$ = observed polarization

I = stationary current along wire

$\hat{n}$ = receiver direction

ζ = displacement along a wire segment

Using equation (2)

$$H(\omega,\Omega) = -jZ_o k_p \sum_{i=1}^{M} u_i R_i \tag{A.2}$$

where

$$R_i = \hat{\varepsilon} \cdot \int \hat{\ell}_i T_i(\zeta) e^{jk_p \frac{\hat{n}\cdot\vec{x}}{L}} \frac{d\zeta}{L} \tag{A.3}$$

In equation (A.3) $\hat{\ell}_i$ is the unit vector of the segment on which $T_i(\zeta)$ is defined. The position $\vec{x}$ can be explicitly written as

$$\vec{x} = \vec{x}_i + \zeta \hat{\ell}_i \tag{A.4}$$

where $\vec{x}_i$ is the position of the beginning end of the segment. Using (A.4) and the basis set of reference [1], the integral in (A.3) can be performed explicitly to obtain

$$R_i = (\hat{\varepsilon}\cdot\hat{\ell}_i)\exp\left(\frac{jk}{L} p\, \hat{n}\cdot(x_i + \zeta_i \hat{\ell}_i)\right) F_i \tag{A.5}$$

The factor F_i takes on one of three values depending on whether i is (a) the beginning point of a segment, (b) not a segment end-point, or (c) the termination point of a segment. The values of F_i for these three cases are, respectively:

$$F_i = \begin{cases} -\alpha^{-1} + f_+(\alpha)/\Delta_i' & \text{(A.6a)} \\ \left(f_+(\alpha) + f_-(\alpha)\right)/\Delta_i' & \text{(A.6b)} \\ -\alpha^{-1} + f_-(\alpha)/\Delta_i' & \text{(A.6c)} \end{cases}$$

where $$f_{(+)}(\alpha) = \left(e^{\alpha\Delta_i'}-1\right)/\alpha^2 \qquad \text{(A.7a)}$$

$$f_{(-)}(\alpha) = \left(e^{-\alpha\Delta_i'}-1\right)/\alpha^2 \qquad \text{(A.7b)}$$

$$\alpha = jk_p \hat{n}\cdot\hat{\ell} \qquad \text{(A.7c)}$$

$$\Delta_i' = \Delta_i/L \qquad \text{(A.7d)}$$

and Δ_i is half the basis width. Comparing (A.2) with (6) we can make the identification

$$G_i = -jZ_o k_p R_i \qquad \text{(A.8)}$$

In accordance with the reduction discussed in reference [1], the vector components G_i' can be formed as follows.

$$G_i' = 0 \qquad \text{(A.9a)}$$

for end points,

$$G_i' = G_i \qquad \text{(A.9b)}$$

for points not adjacent to end points, and

$$G_i' = G_i + \sum_{\ell} G_\ell \ \varepsilon_{\ell i} \qquad \text{(A.9c)}$$

for points adjacent to endpoints. The sum in equation (A.9c) is over all points meeting at the same junction which is adjacent to i. These points (ℓ') are endpoints of all segments meeting at the particular junction. The factor $\varepsilon_{\ell i}$ is

$$\varepsilon_{\ell i} = (-1)\,\frac{\Delta_\ell}{\Delta}\,(-1)^{P_\ell + P_i} + \delta_{\ell i} \qquad \text{(A.9d)}$$

where Δ is the sum over the Δ_ℓ, of all segments meeting at the junction and

$$P_i = \begin{cases} 1 \text{ if adjacent point a beginning point} \\ 2 \text{ if adjacent point a termination point} \end{cases}$$

In practice the G_i' corresponding to endpoints are eliminated since the corresponding rows and columns of $\tilde{Z}'$ are eliminated (see reference [1]).

Again referring to [1] the components of V' can be written as

$$V_i' = \frac{-j4\pi k}{Z_o} p \int \frac{d\zeta}{L}\, T_i(\zeta) \int_o^{2\pi} \frac{d\phi}{2\pi}\; \hat{\ell}_i \cdot \vec{E}_{inc} \qquad \text{(A.10)}$$

where $\vec{E}_{inc}$ is the incident stationary plane wave with wavenumber k_p/L, viz.,

$$\vec{E}_{inc} = \hat{E}_o\, e^{-j \frac{k_p}{L} \hat{m}\cdot\vec{x}} \qquad \text{(A.11)}$$

The magnitude of $\hat{E}_o$ is chosen as unity. For very thin wires variations of $\vec{E}_{inc}$ in the angular integral are negligible and, thus,

$$V_i' = \frac{-j4\pi k}{Z_o} p\, (\hat{E}_o \cdot \hat{\ell}_i) \exp\left(-j\, \frac{k}{L} p\, \hat{m}\cdot(\vec{x}_i + \zeta_i \hat{\ell}_i)\right) Q_i \qquad \text{(A.12a)}$$

where $$Q_i = \left(f_{(+)}(\beta) + f_{(-)}(\beta) \right) / \Delta_i' \qquad \text{(A.12b)}$$

and $$\beta = j\, k_p \hat{m} \cdot \hat{\ell} \quad . \qquad \text{(A.12c)}$$

Once the reduced impedance matrix is obtained for some ω, it can be inverted. The vectors G' and V' can then be calculated as described. The multiplications of equation (8) or (10) can then be performed.

END

FILMED

3-85

DTIC